

Novel Field Effect Transistor Fabrication Based on Non-Graphene 2D Materials

Yu-Tao Li^{1,2}, Hai-Ming Zhao¹, He Tian¹, Peng-Zhi Shao¹, Xin Xin¹, Hui-Wen Cao¹, Ning-Qin Deng¹, Yi Yang¹, Tian-Ling Ren^{*1,2}

¹Institute of Microelectronics & Tsinghua National Laboratory for Information Science and Technology (TNList), Tsinghua University, Beijing 10084, China

²State Key Laboratory of Transducer Technology, Chinese Academy of Sciences
Corresponding Author E-mail: RenTL@tsinghua.edu.cn

ABSTRACT

In this paper, field effect transistors (FET) based on different kinds of non-graphene materials are introduced, which are MoS₂, WSe₂ and black phosphorus (BP). Those devices have their unique features in fabrication process compared with conventional FETs. Among them, MoS₂ FET shows better electrical characteristics by applying a SiO₂ protective layer; WSe₂ FET is fabricated based on a new low pressure chemical vapor deposition (LPCVD) method; BP FET acquires high on/off ratio and high hole mobility by using a simple dry transfer method. Those novel non-graphene materials inspire new design and fabrication process of basic logic device.

INTRODUCTION

Field effect transistor (FET) as the basic logic device plays an important role in information age. Novel two-dimensional (2D) materials show great promise for the next generation low-dimensional FET. However, the FET based on a well-known 2D material, graphene, shows bad on-off ratio due to its zero bandgap property. Therefore, beyond graphene, new kinds of non-graphene materials with reasonable bandgap, such as MoS₂, WSe₂ and black phosphorus (BP), have attracted wide research attention. Unique FET fabrication process was designed for these non-graphene 2D materials to obtain FET with higher mobility and on-off ratio. Here, three works about novel field effect transistor fabrication based on non-graphene 2D materials are presented and discussed.

MoS₂ FETs with a SiO₂ protective layer

A. Introduction

Top-gate MoS₂ FETs with SiO₂ protective layer were fabricated to avoid the monolayer MoS₂ from the influence of charged impurities and interface states by designing unique optical lithography process. As a result, the contact property between the MoS₂ and the electrodes were improved and both the carrier mobility and the source-drain current were enhanced. Comparing with MoS₂ FETs without a SiO₂ protective layer, the SiO₂ protective layer was found to enhance the transfer and output characteristics of MoS₂ FETs. This work applies a practical method to enhance the MoS₂ FETs performance in the low-dimensional FET fabrication process.

B. Monolayer MoS₂ characterization and device fabrication

The details of monolayer MoS₂ growth on SiO₂/Si substrate by CVD method were referred in Ref.1. [1] The AFM image in Figure 1 (a) shows the uniformity of the MoS₂ material with a thickness of ~ 0.71 nm, which accords with the thickness of monolayer MoS₂ well. The red and blue lines in the Figure 1 (b) present the Raman spectrum of MoS₂ material before and after 10 s buffer oxide etching (BOE) process, which are nearly overlapped and indicate that the BOE liquid did not etch the MoS₂ layer. The difference of the two peak in the Ramon spectrum is 19.5 cm⁻¹, which demonstrates the MoS₂ layer is a monolayer.

Two different MoS₂ FETs structures with and without 10 nm SiO₂ protective layer were shown in Figure 1 (c) and (d), respectively. Figure 2 shows the fabrication process of the MoS₂ FETs structure with a SiO₂ protective layer. 10 nm SiO₂ layer was deposited on the MoS₂ surface by ALD to protect the MoS₂ layer from being exposed to the photoresist and other object. By the first lithography step, extra SiO₂ protective layer was etched using 10s BOE process and 25 nm Ti electrodes were deposited on the MoS₂ layer. After the second lithography, the extra SiO₂ and MoS₂ layer were etched by the second BOE process and O₂ plasma, respectively. Finally, the high-k HfO₂ dielectric and Al top gate electrodes were made by conventional fabrication process and MoS₂ FETs structures with SiO₂ protective layer were achieved.

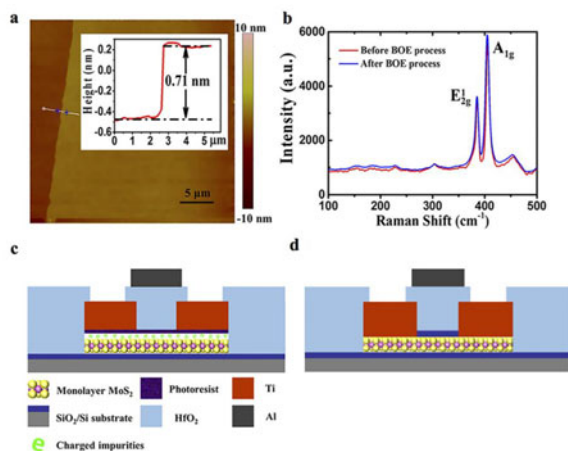


Figure 1. (a) AFM image of the MoS₂ grown on SiO₂/Si substrate by CVD. (b) The Raman spectroscopy measurements on the monolayer MoS₂ material. (c) Schematic perspective view of CVD-grown monolayer MoS₂ FETs without a SiO₂ protective layer. (d) MoS₂ FETs with a SiO₂ protective layer.

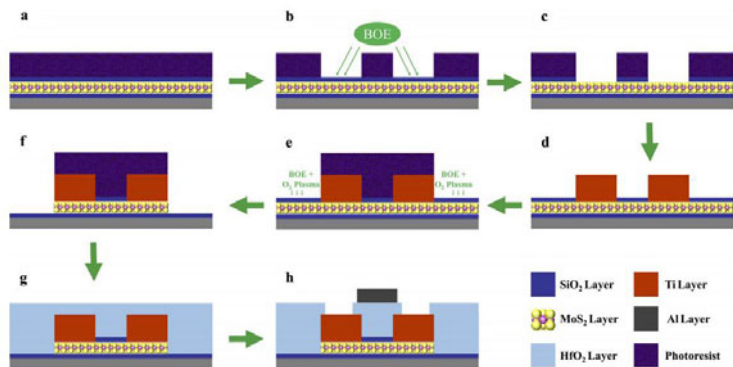


Figure 2. The process of the SiO₂ protective layer technology. (a) Depositing 10nm SiO₂ and coating photoresist on the prepared monolayer MoS₂ material. (b) Patterning the metal electrodes and etched SiO₂ by BOE liquid. (c) The SiO₂ layer was etched. (d) Depositing 25nm Ti metal by lift-off. (e) Etching SiO₂ by BOE liquid and etching MoS₂ material by O₂ plasma. (f) The MoS₂ was etched. (g) Depositing top-gate dielectric 30nm HfO₂ by ALD. (h) Etching the HfO₂ to expose the source/drain electrodes and depositing top-gate electrode Al.

C. Electrical characterization of MoS₂ FETs with a SiO₂ protective layer

Figure 3 shows the measured electronic characteristics of a top-gate monolayer MoS₂ FET with a SiO₂ protective layer, whose channel length and width are both 4 μm. Figure 3 (a) shows the transfer characteristics (red line) of the FET at V_{ds} = 1 V in which the drain-source current (I_{ds}) varies as a function of top-gate voltage (V_{gs}). At V_{ds} = 1 V, the current on/off ratio is ~ 5 × 10⁶ and the FET mobility (μ) calculated by the equation:

$$\mu = \frac{dI_{ds}}{dV_{gs}} \cdot \frac{L}{W} \cdot \frac{1}{C_g \cdot V_{ds}}$$

The FET mobility is ~ 42.3 cm²/V·S, which has increased ~ 20 times compared to the previous MoS₂ FET fabricated without the SiO₂ protective layer.^[2] Figure 4 (b) shows the transfer characteristics at different V_{ds} ranging from 0.025 V to 1 V which exhibits a typical n-type behavior. The output curves shown in the Figure 3 (c) present the saturation properties of the monolayer MoS₂ FET, in which the ohmic contact characteristics can be observed at lower V_{ds}. Compared with the non-ohmic contact in the MoS₂ FET without the SiO₂ protective layer, it can be obviously claimed that the performance of the MoS₂ FET can be largely improved by applying a SiO₂ protective layer.^[2]

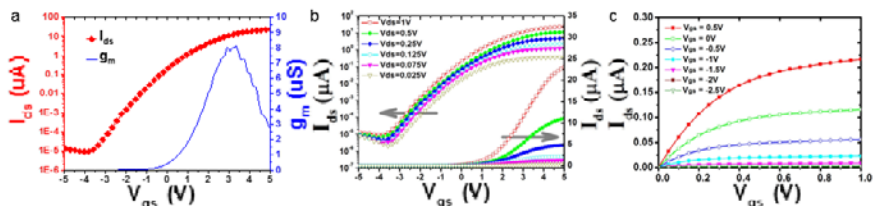


Figure 3. Electrical characterization of MoS₂ FETs with a SiO₂ protective layer. (a) Red curve shows the transfer characteristics of a top-gate CVD grown monolayer MoS₂ FET with SiO₂ protective layer. The blue curve shows the transconductance of the FET. (b) Transfer characteristics of the FET for V_{ds} ranging from 0.025V to 1V. (c) Output characteristics of the FET for the V_{gs} ranging from -2.5V to 0.5V.

WSe₂ FETs based on LPCVD process

A. Introduction

In this work, large-scale growth of high-quality WSe₂ atomic layers directly on SiO₂/Si substrates using a low pressure chemical vapor deposition (LPCVD) method was reported. The influence of growth temperature, carrier gas flow rate and tube pressure was investigated, which affects the sizes, shapes and the thickness of as-grown WSe₂ flakes. By applying a pre-annealing step, the quality of WSe₂ flakes improve a lot which show the lateral size up to 30 μm and monolayer thin film area of 0.25 mm². After that, raman spectrum, microphotoluminescence and auger electron spectroscopy (AES) were performed to characterize the as-grown WSe₂ flakes. Finally, p-type WSe₂ field-effect transistors were fabricated using the WSe₂ flakes which exhibit excellent electrical properties with carrier mobility of ~ 64 cm² · V⁻¹ · s⁻¹ and current on/off ratio over 10⁵. This work opens a new way for the customized low-dimensional non-graphene FET fabrication.

B. Larger scale single crystal WSe₂ growth by LPCVD process

The LPCVD process was performed in a homemade tube furnace with a vacuum pump and pressure meter. After a specific annealing process (see Ref.3 for details), WSe₂ powder (0.2 g) was placed in a quartz boat at the center of a quartz tube, and the clean SiO₂/Si substrates were used as the growth substrate at the downstream with variable temperature. High-purity Argon gas with a designed flow rate was continuously supplied as the carrier gas and the pressure in the tube was pumped down to 10 Pa during the whole growth process. The tube furnace was heated up to 1060 °C in 30 mins and maintained 30 mins for growth. Finally, the whole system was naturally cooled down to ambient temperature.

The as-grown WSe₂ flakes was observed by optical microscope (OM) shown in Figure 4 to Figure 6. Figure 4 shows the influence of temperature on WSe₂ growth, demonstrating larger area flakes begin to appear and merge together with temperature decreasing. However, when the temperature became lower, WSe₂ flakes disappeared and WSe₂ nanoflowers began to form. Figure 5 shows the WSe₂ growth at different tube pressures, indicating suitable lower tube pressure can increase the WSe₂ film size. Figure 6 shows the optical images of the as-grown

WSe₂ flakes under an Ar flow rate of 200 SCCM and the layer number and the domain size of WSe₂ are increased with the increasing of the gas flow rate. Besides, Raman spectrum, microphotoluminescence and auger electron spectroscopy (AES) were performed to characterize the as-grown WSe₂ flakes in Figure 7, which confirm the monolayer, uniformity and chemical composition of the WSe₂ flakes.

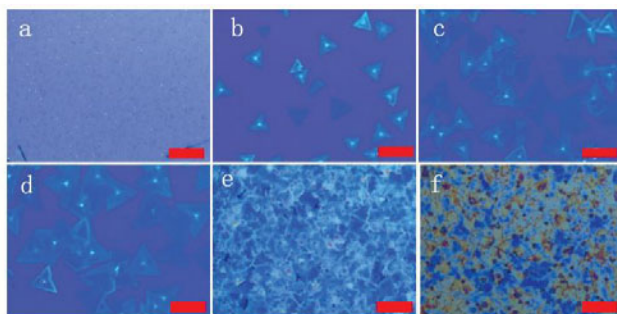


Figure 4. WSe₂ growth with temperatures varying from 850°C to 700°C. Optical microscope images of WSe₂ samples grown at different temperatures under a designed flow rate and vacuum degree (100 SCCM, 200 Pa) for 30 min: (a) 850°C, WSe₂ particles; (b) 800°C, WSe₂ flakes; (c) 780°C, larger WSe₂ flakes; (d) 760°C, larger WSe₂ flakes; (e) 750°C, WSe₂ film and (f) 700°C, WSe₂ nanoflowers. All the scale bars are 20 μm.



Figure 5. Optical images of WSe₂ with different growth pressures: (a) 280 Pa, (b) 180 Pa and (c) 70 Pa. All the scale bars are 20 μm and the temperature used for the pressure dependency study is 765°C.

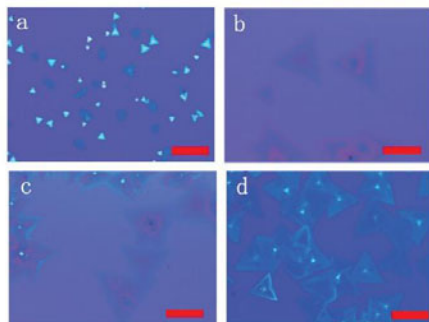


Figure 6. Optical microscope images of large WSe₂ samples grown under an argon flow rate of 200 SCCM for 30 min. From (a) to (d), the temperature decreases from 850 °C to 750 °C. All the scale bars are 20 μm.

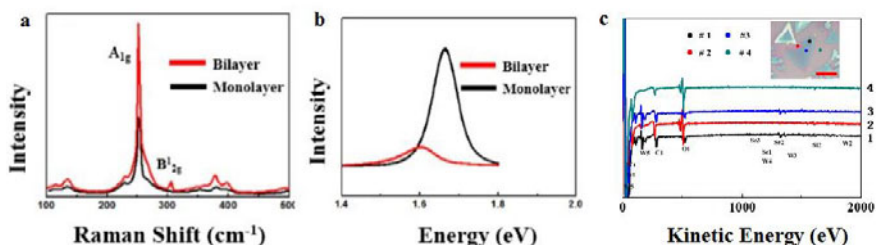


Figure 7. (a) Raman characterization and (b) photoluminescence characterization of monolayer and bilayer WSe₂. (c) AES spectra of the as-grown WSe₂ flakes under an argon flow rate of 200 SCCM at 765 °C for 30 min.

C. Electrical characterization of the monolayer back-gated WSe₂ FET

The as-grown WSe₂ flakes were subsequently used to fabricate back-gated FETs by electronic beam lithography. 5 nm Ti and 25 nm Au were evaporated on the WSe₂ flakes to make the source and drain. Figure 8 shows the transfer curves and output curves of the WSe₂ FETs. The typical I_{SD} - V_{GS} curve in Figure 8 (a) indicates a p-type behavior while the linearity of I_{DS} - V_{DS} curves demonstrates ohmic contacts were formed at the source and drain electrodes. The charge mobility and on/off current ratios of the FETs were $\sim 64 \text{ cm}^2 \cdot \text{V}^{-1} \cdot \text{s}^{-1}$ and 10^5 respectively, which are comparable to the reported results based on exfoliated WSe₂.^[3]

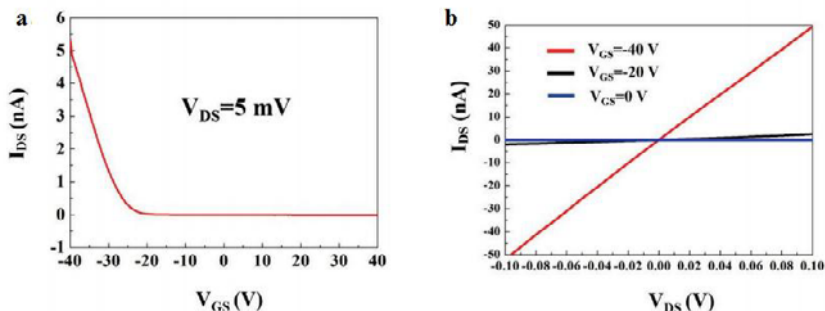


Figure 8. Electrical characterization of the monolayer WSe₂ based back-gated FET device. (a) I_{DS} - V_{GS} plots of back-gated FET at $V_{DS} = 5$ mV. (b) I_{DS} - V_{DS} output characteristics at $V_{GS} = 0$, -20V and -40 V.

BP FET based on a simple dry transfer method

A. Introduction

An as-prepared BP FET was fabricated using a simple dry transfer method to minimize polymer residues and avoid the liquid immersion process compared with conventional material transfer process. As a result, BP with little degradation was achieved while the BP FET exhibited excellent electrical properties with a relatively high on/off ratio of 10^4 and a high hole mobility exceeding $380 \text{ cm}^2/(\text{V} \cdot \text{s})$. Besides, due to the degradation and doping effect, BP shows a time-dependent electrical property indicating the declining and recovering process. Finally, it was demonstrated that the degradation and large-scale hysteresis of BP FET could be modified by covering a thin Al₂O₃ layer.

B. BP characterization and device fabrication

The details of BP using a simple dry transfer method were referred in Ref.4^[4]. The AFM image in Figure 9 (a) shows the uniformity of the dry-transferred BP with a thickness of only 5 nm, demonstrating the transfer technique performed well. However, the three obvious peaks (A_{1g} , B_{2g} , and A_{2g}) of the Raman spectrum in Figure 9 (b) indicate that the dry transferred BP is not monolayer.^[6]

The all-dry transfer process for fabricating BP FET is shown in Figure 10. Firstly, thin-layer BP was exfoliated onto a transparent poly (vinyl chloride) (PVC) film and adhered the film to the micromanipulation platform. After that, the few-layer BP was transferred onto the stripe-shaped electrodes on the Si/SiO₂ substrate by pressing the PVC film down. Finally, lift up the film and the target BP was left on the electrodes to achieve a BP FET with bottom electrodes. It is worth noting that the air exposure time should be limited to 10 min during the fabrication and an annealing process is necessary to improve the contact between electrodes and BP, in which the sample is heated at 200 °C in an argon environment for 20 min.

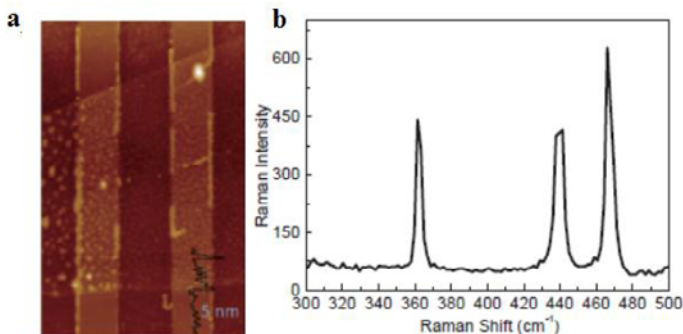


Figure 9. (a) AFM image of the BP using a simple dry transfer method. (b) The Raman spectroscopy measurements on the BP material.

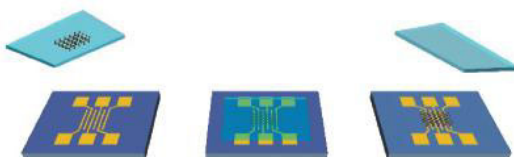


Figure 10. The all-dry transfer process for fabricating BP FET.

C. Electrical characterization of BP FET

The electrical property of BP FET was measured in ambient atmosphere shown in Figure. 11. The on-state current reached up at 0.01 V drain bias and the on/off ratio exceeded 10^4 . The hole mobility was calculated up to $380 \text{ cm}^2/(\text{V} \cdot \text{s})$, which is comparable to those in other related literatures where BP FET was fabricated in a glove box or measured in vacuum. ^[5] Figure. 11 (b) shows the output characteristic of BP FETs ^[6]. For a negative back gate voltage, the current tends to saturate at a high drain bias because of pinch-off. However, the drain current exhibited Schottky behavior when the back gate voltage was more than 0 V, which was demonstrated in other work as well. ^[5]

Figure 12 (a) shows the transfer curve measured under different times, indicating that the electrical conduction of BP was quickly changed from declining to recovering. After depositing a Al_2O_3 protection layer, the transfer curves of BP FET with initial state and 150 min exposure to ambient atmosphere were shown in Figure 12 (b) and (c). The limited changes in the two curves demonstrate the excellent protective function of Al_2O_3 layer. This research has great significance to the fundamental researches and applications of BP. ^[4]

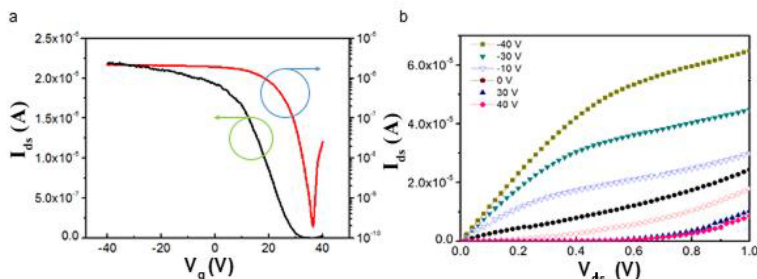


Figure 11. (a) The transfer curve at 0.01 V drain bias. The black and red curves are plotted in linear and logarithmic scales, respectively. (b) The output characteristic of BP FETs under different gate voltages.

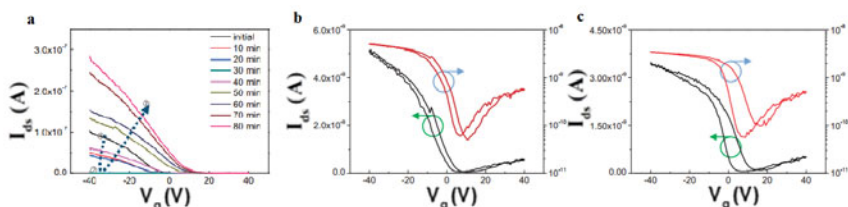


Figure 12. (a) Time-dependent electrical property of BP FET. The dashed arrow shows the change in electrical property. (b) Transfer curve of BP FET with 30 nm Al_2O_3 as protection layer. (c) Transfer curve after 150 min exposure to ambient atmosphere of the same FET.

CONCLUSIONS

Three works related to non-graphene 2D materials FETs are presented in this paper. The inserted SiO_2 protective layer enhances the carrier mobility and the source-drain current of MoS_2 FETs. And larger scale single crystal WSe_2 growth by LPCVD process shows the potential to fabricate wafer-scale logic circuits. Moreover, BP FET based on a simple dry transfer method provides a process to improve the performance of the device based on unstable materials. These novel non-graphene based FETs processes inspire new design of basic logic device and their application in electronic systems.

ACKNOWLEDGMENTS

This work was supported by the National Natural Science Foundation (61574083, 61434001), National Basic Research Program (2015CB352101), National Key Research and Development Program (2016YFA0200400), National Key Project of Science and Technology (2011ZX02403-002), Special Fund for Agroscientific Research in the Public Interest (201303107) of China, and Research Fund from Beijing Innovation Center for Future Chip. The authors are also thankful for the support of the Independent Research Program (2014Z01006) of

Tsinghua University, and Advanced Sensor and Integrated System Lab of Tsinghua University Graduate School at Shenzhen (ZDSYS20140509172959969).

REFERENCES

1. J. Zhang, H. Yu, W. Chen, X. Tian, D. Liu, M. Cheng, G. Xie, W. Yang, R. Yang, and X. Bai, *ACS Nano* 8, 6024 (2014).
2. P. Z. Shao, H. M. Zhao, H. W. Cao, X. F. Wang, Y. Pang, Y. X. Li, N. Q. Deng, J. Zhang, G. Y. Zhang, Y. Yang, S. Zhang, and T. L. Ren, *Appl. Phys. Lett.* 108, 203105 (2016).
3. H. W. Cao, H. M. Zhao, X. Xin, P. Z. Shao, H. Y. Qi, M. Q. Jian, Y. Y. Zhang, Y. Yang, and T. L. Ren, *Mod. Phys. Lett. B* 30, 1650267 (2016).
4. X. Xin, H. M. Zhao, H. W. Cao, H. Tian, Y. Yang, and T. L. Ren, *Appl. Phys. Express* 9, 045202 (2016).
5. L. Li, Y. Yu, G. J. Ye, Q. Ge, X. Ou, H. Wu, D. Feng, X. H. Chen, and Y. Zhang, *Nat. Nanotechnol.* 9, 372 (2014).
6. W. Lu, H. Nan, J. Hong, Y. Chen, C. Zhu, Z. Liang, X. Ma, Z. Ni, C. Jin, Z. Zhang, *Nano Res.* 7, 853 (2014).